INORGANIC CHEMISTRY FRONTIERS

CCS 中国化学会 CHINESE CHEMICAL SOCIETY

ROYAL SOCIETY OF CHEMISTRY

Enhanced Deep Red to Near-Infrared (DR-NIR) Phosphorescence in Cyclometalated Iridium(III) Complexes

Journal:	*Inorganic Chemistry Frontiers*
Manuscript ID	QI-RES-09-2022-002058.R1
Article Type:	Research Article
Date Submitted by the Author:	30-Oct-2022
Complete List of Authors:	Yoon, Sungwon; University of Houston Teets, Thomas; University of Houston

ARTICLE

Enhanced Deep Red to Near-Infrared (DR-NIR) Phosphorescence in Cyclometalated Iridium(III) Complexes†

Received 00th January 20xx,
Accepted 00th January 20xx

DOI: 10.1039/x0xx00000x

Sungwon Yoon [a] and Thomas S. Teets*[a]

The design of deep-red to near-infrared (DR-NIR) phosphorescent compounds with high photoluminescence quantum yields (Φ_{PL}) is a significant fundamental challenge that impacts applications including optoelectronic devices, imaging, and sensing. Here we show that bis-cyclometalated iridium complexes with electron-rich ancillary ligands can have exceptional quantum yields for DR-NIR phosphorescence (peak λ > 700 nm). Six bis-cyclometalated iridium(III) complexes with DR-NIR phosphorescence are described in this work, pairing highly conjugated cyclometalating ligands with electron-rich and sterically encumbered β-ketoiminate (acNac), β-diketiminate (NacNac), and *N*,*N*′-diisopropylbenzamidinate (dipba) ancillary ligands. The photoluminescence spectra and quantum yields are solvent-dependent, consistent with significant charge-transfer character in the emissive excited state. The ancillary ligands perturb the excited-state kinetics relative to closely related compounds, which can lead to enhanced Φ_{PL} values in the DR-NIR region, particularly in toluene solution and in doped polymer films.

Introduction

Materials emitting in the near-infrared (NIR) region (ca. 700–2500 nm) have aroused interest for applications in several areas,[1] including night vision and surveillance technologies, information security, optical communications,[2] bioimaging,[3–5] and photodynamic therapy.[6–8] As the applications of NIR-emitting materials continually expand, there is a growing demand for new solution-processible materials with advanced performance in flexible and wearable devices. Therefore, several types of novel NIR-emitting materials are being studied, primarily organic dyes,[9] quantum dots (QDs),[10] and transition metal-based phosphors.[11,12] Among transition metal-based phosphors, there are many that luminesce at the boundary between the red and near-infrared regions, between ca. 700–800 nm, which will be termed herein as deep-red to near-infrared (DR-NIR). State-of-the-art examples are described here and summarized in Table S1 of the ESI.† Platinum(II) and osmium(II) complexes have been the most efficient DR-NIR emitters (ca. 700–900 nm).[13–19] A state-of-the-art electroluminescent device with λ_{em} = 740 nm and a record external quantum efficiency (EQE) of 24% was obtained from a Pt(II) complex, $Pt(fprpz)_2$ (fprpz = 5-(2-pyrazinyl)-3-trifluoromethylpyrazolate) that also exhibits high photoluminescence quantum yield (Φ_{PL}) of 81% in neat film.[14] There are examples of diplatinum complexes with short Pt···Pt interactions that luminesce efficiently in the DR-NIR.[18,19] Meanwhile, Os(II) complexes tend to have pure metal-to-ligand charge transfer (MLCT) excited states and diminished intermolecular interactions due to their octahedral configuration, which removes the requirement of neat films and allows efficient phosphorescent emission in dilute films for $Os(ftrmpz)_2(PPhMe_2)_2$ (ftrmpz = 5-(3-(trifluoromethyl)-1*H*-1,2,4-triazolato-5-yl)pyrazine), with EQE of 11.5% at λ_{em} = 710 nm.[16] A complementary approach to molecular DR-NIR phosphors involves spin-flip emission in Cr(III) complexes, producing long-lived DR-NIR emission with good quantum yields.[20–22] As impressive as these outcomes are, there is a demand for further development of novel DR-NIR luminescent materials for these applications.

Phosphorescent cyclometalated iridium(III) complexes are one of the most widely explored classes of molecular phosphors, contributing to various applications in sensing,[23] photoredox catalysis,[24] light-emitting electrochemical cells (LEECs),[25] and organic light-emitting diodes (OLEDs).[26–29] Whereas homoleptic complexes of type *fac*-$Ir(C^N)_3$ (C^N = cyclometalating ligand) are a popular option for both photocatalysis and OLEDs, heteroleptic complexes of the $Ir(C^N)_2(L^X)$ (L^X= ancillary ligand) structure type are also becoming prominent since the ancillary ligands not only can help tune the emission color, but also perturb the excited-state dynamics. The key features of these iridium(III) complexes include facile color tunability, high photoluminescence quantum yields (Φ_{PL}), and relatively short phosphorescence lifetimes (τ) along with good thermal and photostability.[30]

Designing DR-NIR-phosphorescent materials with high Φ_{PL} is intrinsically more difficult, and a survey of the literature on cyclometalated iridium complexes makes this challenge clear.

[a] *University of Houston, Department of Chemistry, 3585 Cullen Blvd., Room 112, Houston, TX 77204-5003, USA.*
Email: tteets@central.uh.edu

† Electronic Supplementary Information (ESI) available: Experimental details, X-ray crystallography details, UV-vis absorption spectra, additional PL and excitation data, and NMR spectra. See DOI: 10.1039/x0xx00000x

Whereas there are previously discovered red-phosphorescent cyclometalated iridium compounds with Φ_{PL} ~ 0.5 in solution,[27,31,32] it is rare to find DR-NIR analogues with Φ_{PL} > 0.2.[33–35] The quantum yield is defined as the ratio of emitted photons to absorbed photons and can be expressed as the ratio of the radiative rate constant (k_r) to the sum of radiative and nonradiative (k_{nr}) rate constants. In DR-NIR emitters k_{nr} increases due to greater vibrational overlap between the ground and excited states based on the energy gap law,[36,37] whereas k_r is expected to be smaller due to a cubic dependence on the transition energy.[38] Recent notable advances in DR-NIR-phosphorescent iridium complexes have focused on modifications to the cyclometalating ligand, including complexes supported by substituted 1-phenylisoquinline (piq) analogues with emission beyond 700 nm,[34] and complexes with a "core-shell" cyclometalating ligand design that combines a rigid, conjugated core ligand with a flexible, electron-rich thienyl or diphenylamino shell.[35]

Our group has tackled the above-mentioned challenges in the red (λ_{em} = 600–650 nm)[39,40] and deep-red regions (λ_{em} = 650–700 nm)[41,42] with a new class of bis-cyclometalated iridium phosphors. We have demonstrated that electron-rich, π-donating ancillary ligands strongly perturb the metal-centered HOMO and increase the metal *d*-orbital participation in the excited state, resulting in augmented k_r and in some cases Φ_{PL} values. With this strategy, we have achieved solution Φ_{PL} values as high as 0.8 in the red region of the spectrum,[39] and eclipsed Φ_{PL} = 0.5 in the deep red region.[41] Another insight to emerge from these previous works is that the nature of the C^N ligand plays a major role in the effectiveness of this approach. In general, the phosphorescence in complexes where the C^N ligands have electron-rich thiophene-based cyclometalated aryl groups is minimally influenced by the ancillary ligand, whereas with phenyl-based C^N ligands the phosphorescence wavelength and k_r values are both strongly responsive to how electron-rich the ancillary ligand is.

In this work we use the above-mentioned insights to design high-performing DR-NIR emitters, achieving some of the highest DR-NIR Φ_{PL} values ever reported for cyclometalated iridium complexes. The two cyclometalating ligands we use are phenyl-substituted highly conjugated heterocycles, known to engender phosphorescence with long wavelengths.[34,43] The electron-rich ancillary ligands are chosen among the ones previously used in our group that resulted in increased quantum yields in the red and deep-red regions.[39,41] A total of six new compounds are described in this paper. Cyclic voltammetry reveals the effects of the electron-rich ancillary ligands on the HOMO energies, and detailed photophysical analysis in three solvents (MeCN, THF and toluene) and in transparent polymer film catalogues the effects on the excited-state dynamics and Φ_{PL}. In general, we observe the highest solution quantum yields in the less polar toluene solvent, including one example with Φ_{PL} = 0.53 and λ_{em} = 709 nm, one of the highest recorded for a DR-NIR cyclometalated iridium complex. This work shows that electron-rich ancillary ligands are an effective design element for top-performing DR-NIR emitters, a region of the spectrum where quantum yields are typically modest.

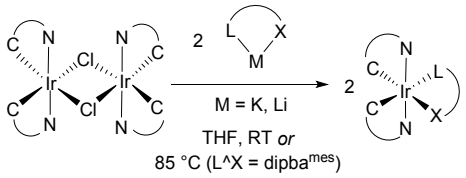

1 C^N = pphen, L^X = acNac
2 C^N = pphen, L^X = NacNac
3 C^N = pphen, L^X = (Cy)acNac
4 C^N = piqCN, L^X = acNac
5 C^N = piqCN, L^X = (dmp)$_2$NacNac
6 C^N = piqCN, L^X = dipba^{mes}

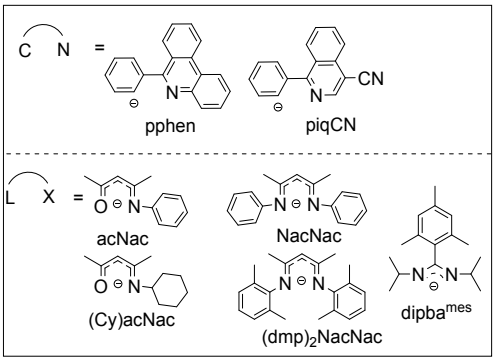

Scheme 1. Synthesis of the iridium(III) complexes.

Results

Synthesis and Structural Characterization. The general synthetic procedure for six new complexes of the general form Ir(C^N)$_2$(L^X) (C^N = 6-phenylphenanthridine (pphen) or 1-phenylisoquinoline-4-carbonitrile (piqCN)) is described in Scheme 1. The cyclometalating ligands are chosen to engender the complexes with emission in the DR-NIR region of the spectrum[34,43] by adding additional π conjugation (pphen) or a cyano group (piqCN) to 1-phenylisoquinoline (piq), a ubiquitous C^N ligand in red-phosphorescent iridium complexes.[31,32,39,41] These C^N ligands are paired with five ancillary ligands (L^X) previously used in studies of red and deep-red emitters. Besides β-ketoiminate (acNac) and β-diketiminate (NacNac) ancillary ligands that we have extensively worked with,[39,44,45] the more sterically encumbered NacNac ((dmp)$_2$NacNac) and amidinate (dipba^{mes}), and more electron-rich acNac ((Cy)acNac) are included in this study.[41] To prepare the complexes, [Ir(C^N)$_2$(μ-Cl)]$_2$ was treated with the potassium or lithium salts of the appropriate ancillary ligand in tetrahydrofuran at room temperature or 85 °C.[41,46] Some combinations of C^N and L^X ligands resulted in intractable product mixtures that we were unable to purify, but the complexes shown in Scheme 1 were obtained in pure form with isolated yields ranging between 25% and 60%. The identity and purity were validated by ^{1}H and ^{13}C{^{1}H} NMR spectroscopy (Fig. S38–S49†) and mass spectrometry. The NMR spectra clearly reveal the differences in symmetry between the NacNac, (dmp)$_2$NacNac and dipba^{mes} complexes (all C_2), and the C_1-symmetric acNac and (Cy)acNac analogues.

Complexes **1** and **6** were characterized by single-crystal X-ray diffraction.§ The structures of the complexes are shown in Fig. 1, and detailed crystallographic data reported in Table S2†.

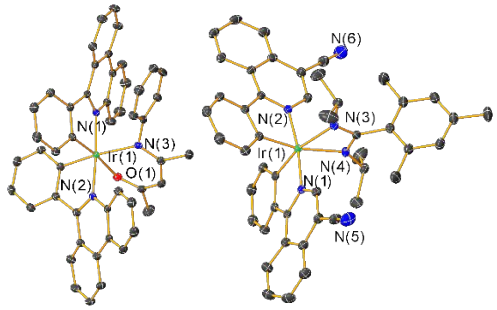

Fig. 1. X-ray crystal structures of complexes **1** (left) and **6** (right). Ellipsoids are depicted at 50% probability with hydrogen atoms and solvent molecules omitted.

In all the structures, an approximately octahedral geometry about the iridium(III) center is observed, and a trans disposition of the two nitrogen atoms of the cyclometalating ligands is revealed as typically found in bis-cyclometalated iridium complexes. In **6** the core of the dipba^{mes} ancillary ligand is planar, with the mesityl ring nearly orthogonal to the core. In **1** we observe a more significant buckling of the acNac ancillary ligand than normal,[39,44] to accommodate the more sterically crowded environment brought on by the phenanthridine heterocycles. The pphen ligands themselves are twisted in the structure of **1**, to enable cyclometalation and provide a large enough cleft for the acNac ancillary ligand. Otherwise, structural metrics in **1** and **6** are unremarkable and are similar to other related structures.[39,41,42,44] Crystal packing in these compounds seems to involve nonspecific van der Waals interactions between neighboring molecules and nearby solvate molecules.

Electrochemistry. The electrochemical properties of all complexes were investigated by cyclic voltammetry (CV) in acetonitrile solution. In most bis-cyclometalated iridium(III) complexes, the lowest unoccupied molecular orbital (LUMO) is located on the C^N ligands while the highest occupied molecular orbital (HOMO) has a more complex nature.[47] In previous DFT calculations on an Ir(piq)$_2$(L^X) series closely related to **1**–**6**, we found that >95% of the LUMO density is on the C^N ligands, mainly the *N*-heterocycles.[39] The HOMO is mainly delocalized over Ir and the C^N ligand when L^X =

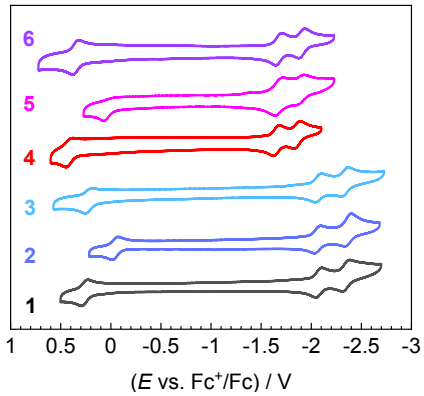

Fig. 2. Overlaid cyclic voltammograms of complexes **1**–**6** were recorded at 0.1 V/s in MeCN with 0.1 M TBAPF$_6$ supporting electrolyte. Potentials are referenced to an internal standard of ferrocene, and currents are normalized to bring all the traces to the same scale.

Table 1. Summary of cyclic voltammetry data for complexes **1**–**6**.[a]

Complex	(*E* vs. Fc$^+$/Fc) / V		*E* / eV[c]		
	E^{red}	E^{ox}	HOMO	LUMO	ΔE_{H-L} / eV[d]
1	−2.08, −2.35	+0.26	−5.1	−2.7	2.34
2	−2.06, −2.37	−0.04	−4.8	−2.7	2.06
3	−2.07, −2.34	+0.22	−5.0	−2.7	2.29
4	−1.65, −1.86	+0.41	−5.2	−3.2	2.06
5	−1.68, −1.89	0.00[b]	−4.8	−3.1	1.68
6	−1.68, −1.91	+0.35	−5.2	−3.1	2.03

[a] Measured in MeCN at room temperature, with 0.1 M (NBu_4)(PF_6) electrolyte, using a glassy carbon working electrode, platinum wire counterelectrode, and silver wire pseudoreference electrode. Potentials are referenced to an internal standard of ferrocene. [b] Irreversible wave ($i_{p,a}/i_{p,c}$ <<1). Reported potential is the half-peak potential.[48] [c] Absolute frontier orbital energies, estimated from the equation $E = -[(E \text{ vs. } Fc^+/Fc) + 4.8]$ using E^{ox} (HOMO) and the first E^{red} (LUMO).[49,50] [d] Electrochemical HOMO–LUMO gap, estimated as $E^{ox} - E^{red}$.

acetylacetonate (acac), but involves progressively more L^X character as the ancillary ligand is made more electron-rich, 36% for acNac, 62% for dipba, and 80% for NacNac. The redox behavior of **1**–**6** suggest very similar frontier orbital localization in these compounds. As shown in Fig. 2 and Table 1, two reversible one-electron reduction waves are observed in all complexes resulting from a sequential population of π* orbitals on each C^N ligand. Comparing complexes with the same C^N ligand, the potential for the first reduction depends minimally on the identity of the ancillary ligand, occurring between –2.06 and −2.08 V vs. ferrocenium/ferrocene (Fc$^+$/Fc) for C^N = pphen (**1**–**3**), and −1.65 and −1.68 V for C^N = piqCN (**4**–**6**). Notably, these potentials are all > 120 mV (C^N = pphen) or > 550 mV (C^N = piqCN) more positive than the less-conjugated C^N = piq analogues,[39,41] indicating that the increased C^N ligand conjugation in **1**–**6** has a significant stabilizing effect on the LUMO energy.

In contrast, the Ir^{IV}/Ir^{III} potentials (E^{ox}) strongly depend on the identity of the ancillary ligands. Reversible waves are observed for all the complexes except for **5**. Complexes **2** and **5**, containing NacNac, have very similar oxidation potentials (E^{ox} = −0.04 and 0.00 V, respectively), right at the Fc$^+$/Fc couple. By replacing one oxygen in acNac with one *N*-phenyl group going from **1** to **2**, a cathodic shift of *ca*. 0.2 V is observed. Complex **3**, with the more basic (Cy)acNac, has an Ir^{IV}/Ir^{III} potential shifted by only 40 mV relative to complex **1**, suggesting that the basicity of the acNac nitrogen donor has only a small influence on the redox potential. Another observation is that the complex with a smaller bite angle ancillary ligand (**6**) is more difficult to oxidize than the NacNac complexes, by 0.35 V, which we attribute to less π donation into the d orbitals caused by the poorer overlap between ligand orbitals and the metal dπ orbitals. Overall, the results indicate that the L^X ligand strongly affects the energy of HOMO, while not perturbing the LUMO energy much. As a result, the HOMO–LUMO gap and corresponding charge-transfer excited-state energy decrease as the ancillary ligand is made more electron-rich, a concept that manifests itself in the photoluminescence spectra (see below).

Photophysical Properties. The UV-vis spectra of all complexes were recorded in THF at room temperature and depicted in Fig. S1–S4†. In the absorption spectra of complexes **1**–**6**, intense

absorption bands with large molar absorptivity values (ε = 5–40 × 10^3 $M^{-1}cm^{-1}$) in the UV region are assigned to spin-allowed ligand-centered (LC) π→π* transitions of the cyclometalating and ancillary ligands.[27,51] Weaker, overlapping absorption bands tailing beyond 500 nm are assigned as both singlet and triplet mixed metal-ligand-to-ligand charge transfer ($^{1/3}$MMLL'CT) transitions. In general, the spectra are minorly perturbed by the ancillary ligand within the same type of cyclometalating ligand. The normalized spectra in Fig. S2 and S4† more clearly show the subtle differences in the longer-wavelength regions brought on by the different L^X regions. Some noticeable differences were observed in complexes **2** and **6**. In complex **2** using L^X = NacNac, an absorption shoulder near 400 nm is noted, which is assigned to a NacNac centered π-π* transition.[45] Complex **6,** using L^X = dipba^{mes}, displays an additional well-resolved band around 530 nm. A similar feature was observed in previously described complexes with dipba^{mes} and related amidinate or guanidinate ancillary ligands,[39,41] although it occurs at shorter wavelength, below 500 nm, when C^N = piq. We assign this band to a spin-allowed HOMO→LUMO charge-transfer transition, shifted to lower energy in **6** because of the stabilized HOMO in piqCN (see above description of electrochemistry and frontier orbitals). The higher osicillator strength when L^X = dpiba^{mes} is likely a reflection of the different π orbital symmetry in the HOMO between dipba and (N)acNac.[39]

All of complexes **1**–**6** are luminescent in fluid solution at room temperature. Steady-state photoluminescence spectra and quantum yields were recorded in three solvents of varying polarity, MeCN (ε = 36.64), THF (ε = 7.52), and toluene (ε = 2.38). Spectra overlaid in the three solvents are shown in Fig. S5–S10 of the ESI†, and the data are summarized in Table S3†. In four of the six compounds, except for acNac complexes **1** and **4,** the PL is blue-shifted in the more polar MeCN solvent relative to THF and toluene. We note that while it is common in cyclometalated iridium complexes to see PL maxima shift to longer wavelengths with increasing polarity, i.e. positive solvatochromism,[52,53] the solvatochromic behavior in these compounds is more irregular, and may also be influenced by solvent viscosity[54] or other effects. Nevertheless, the sizeable shifts of the PL spectra with changing solvent polarity are consistent with significant charge-transfer character in the emissive excited states.[54,55] In charge-transfer excited states there are significant changes in dipole moments between the ground-state and excited state, so the relative energies of these two states, and thus the PL that results, are dependent on the polarity of the medium. Moreover, photoluminescence quantum yields (Φ_{PL}) of **1**–**6** tend to increase as the solvent polarity decreases (Table S3†). Excitation spectra of the complexes were collected in THF and toluene and shown in Fig. S11–S22†. For all complexes, the excitation and absorption spectra are superimposed, indicating that the emission signal originates from the iridium complex and not from an impurity, and that the same T_1 state is populated regardless of excitation wavelength, in accordance with Kasha's rule.

Since the highest quantum yields were observed in toluene, we focused most of our attention on the photoluminescence properties in this solvent and discuss those data in detail here. The spectra recorded in toluene are shown in Fig. 3, with major spectroscopic characteristics summarized in Table 2. All complexes have room-temperature emission in the DR-NIR region, with emission maxima occurring near or beyond 700 nm, and all are red-shifted compared to the reference Ir(piq)$_2$(L^X) complex at parity of ancillary ligand, by at least 43 nm (930 cm^{-1}) when measured in the same solvent, THF (see Table S1†).[39,41] For a given C^N ligand the emission maxima are strongly dependent on the ancillary ligand, with the complexes Ir(pphen)$_2$(NacNac) (**2**) and Ir(piqCN)$_2$(dipba^{mes}) (**6**) exhibiting the longest-wavelength emission bands in the series. In toluene, the photoluminescence quantum yields are enhanced by as much as a factor of 4 relative to the more polar solvents (see Table S3). The absolute highest Φ_{PL} value in toluene is 0.53 for Ir(piqCN)$_2$(acNac) (**4**), which represents one of the highest values recorded for a DR-NIR cyclometalated iridium complex in solution. The quantum yields of Ir(pphen)$_2$(acNac) (**1**, Φ_{PL} = 0.27) and Ir(piqCN)$_2$(dipba^{mes}) (**6**, Φ_{PL} = 0.30) are also very good for the DR-NIR region.[57] The lifetimes (τ) of the excited state at room temperature are sub-microsecond and in general less responsive to the change in solvent, ranging between 0.12–0.89 μs in THF and 0.21–0.95 μs in toluene (see Fig. S23–S28† for the time-resolved PL decay traces in toluene). The higher quantum

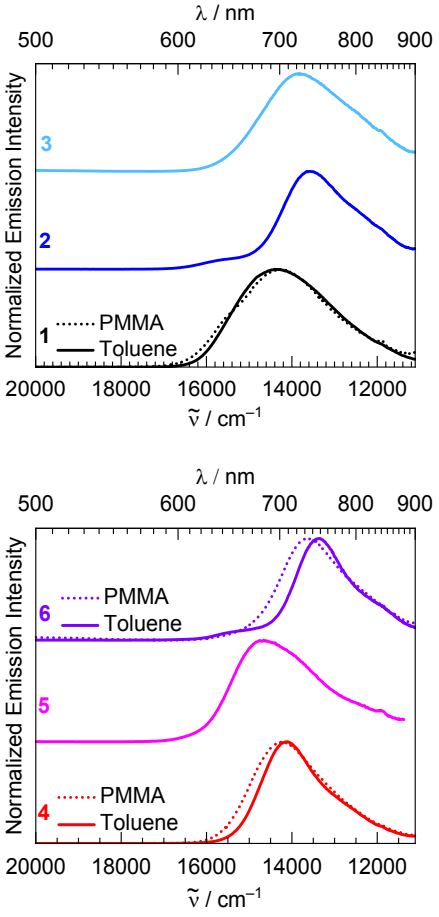

Fig. 3. Stacked room temperature emission spectra of complexes with (a) C^N = pphen (**1**–**3**), and (b) C^N = piqCN (**4**–**6**) in toluene. The spectra of **1**, **4**, and **6** were also recorded in 2 wt% PMMA films and are overlaid as dotted lines. Samples were excited at λ_{ex} = 420 nm.

Table 2. Summary of room-temperature photoluminescence data for complexes **1**–**6** in toluene.

Complex	λ_{em} / nm[a]	Φ_{PL}[b]	τ / μs[c]	($k_r \times 10^{-5}$ / s^{-1}) / ($k_{nr} \times 10^{-5}$ / s^{-1})[d]
1	694	0.27	0.95	2.8 / 7.7
2	736	0.080	0.21	3.8 / 44
3	723	0.095	0.38	2.5 / 24
4	709	0.53	0.53	10 / 8.9
5	682	0.10	0.60	1.7 / 15
6	749	0.30	0.22	14 / 32

[a] Excited at 420 nm. [b] Measured via a relative method, using tetraphenylporphyrin in toluene (Φ_{PL} = 0.11)[56] as the standard. [c] Excited at 390 nm. [d] $k_r = \Phi_{PL}/\tau$, $k_{nr} = (1-\Phi_{PL})/\tau$, assuming 100% population of the emissive T_1 state.

yields in toluene are a combination of radiative and nonradiative effects. Except for complex **3**, which has nearly identical Φ_{PL} in THF and toluene, the rest all have higher k_r values in toluene, and all but complex **5** have smaller k_{nr} values in toluene (see Table S3†).

The photoluminescence spectra were also recorded in a frozen toluene glass at 77 K (Fig. S29–S34†). The two distinct vibronic maxima become sharper and better resolved for most of the complexes. Compared to the room temperature spectra, we can observe measurable rigidochromic blue shifts, similar for all complexes and ranging between 18–32 nm (330–640 cm^{-1}), depending somewhat on the ancillary ligand, which in concert with the above-mentioned solvatochromism suggests significant charge-transfer character in the excited state.[58]

To further study the photophysical properties in a more device-relevant medium, the photoluminescence data of the best-performing compounds in this series (**1**, **4**, and **6**) were measured in PMMA (PMMA = poly(methyl methacrylate)) films. The sample films were fabricated inside of a glovebox by dissolving 2 wt% of the emitter and PMMA in dichloromethane, drop-coating the solution onto a quartz slide, and drying by evaporation. The spectra of these three compounds in PMMA are included in Fig. 3, and the data summarized in Table 3. Fig. S35–S38† display the time-resolved PL decay traces of the PMMA samples. In all cases the peak wavelengths are modestly shifted from those recorded in toluene, by no more than 15 nm (270 cm^{-1}) . Compared to solution, complexes with L^X = acNac showed an increase in quantum yield relative to solution values, with Φ_{PL} = 0.65 in PMMA and 0.27 in toluene (complex **1**), and Φ_{PL} = 0.79 in PMMA and 0.53 in toluene (complex **4**). These increases in Φ_{PL} are due to increases in k_r and decreases in k_{nr}, with longer lifetimes observed in the PMMA films (τ = 1.1 μs for **1** and 0.74 μs for **4**). In contrast, the quantum yield of dipba^{mes} complex **6** decreased from 0.30 in toluene solution to 0.14 in PMMA film.

Table 3. Summary of room-temperature photoluminescence data for complexes **1**, **4**, and **6** at 2 wt% in PMMA film.

Complex	λ_{em} / nm[a]	Φ_{PL}[b]	τ / μs[c]	($k_r \times 10^{-5}$ / s^{-1}) / ($k_{nr} \times 10^{-5}$ / s^{-1})[d]
1	700	0.65	1.1	5.9/3.2
4	702	0.79	0.74	11/2.8
6	734	0.14	0.33	4.2/26

[a] Excited at 420 nm. [b] Absolute quantum yield, measured using an integrating sphere. [c] Excited at 390 nm. [d] $k_r = \Phi_{PL}/\tau$, $k_{nr} = (1-\Phi_{PL})/\tau$, assuming 100% population of the emissive T_1 state.

Discussion

Here we show that electron-rich ancillary ligands can support bis-cyclometalated iridium complexes with among the highest DR-NIR phosphorescence quantum yields reported (see Table S1 for comparisons to other notable literature examples). Before our entry into this area, some of the top-performing DR-NIR phosphors were of analogues of Ir(btph)$_2$(acac), where btph is the cyclometalating ligand 6-(3-benzothiophenyl)phenanthridine, which combines a benzothiophene cyclometalated aryl with a phenanthridine heterocycle, and acac is acetylacetonate. Compounds of this type typically have Φ_{PL} ~ 0.3 with peak emission wavelengths near 720 nm.[33] Our initial attempts to improve DR-NIR quantum yields involved pairing btph with rigid quinoline-based ancillary ligands[46] or the types of electron-rich ancillary ligands we used in this work.[42] However, we found that the excited-state dynamics in these bis-cyclometalated btph complexes were generally unresponsive to the ancillary ligand, and we were only able to achieve similar outcomes or slight improvements over the parent Ir(btph)$_2$(acac) precedent.

As a result, we determined that to use electron-rich ancillary ligands to improve the efficiency of DR-NIR phosphors, as we had successfully done in the red region, we would need cyclometalating ligands where the cyclometalated aryl group is a simple phenyl ring, in which case the T_1 excited state has higher MLCT character and is much more responsive to the ancillary ligand structure. We had previously established this concept in a series of red and deep-red phosphorescent compounds,[39,41] and insight from other groups also lends credence to this design criterion. MLCT character in the triplet excited state can be quantified by measuring zero-field splitting (ZFS), which has been done with several cyclometalated iridium complexes, mainly in the *fac*-Ir(C^N)$_3$ and Ir(C^N)$_2$(acac) structural classes.[47] In those compounds, ZFS values for C^N ligands with cyclometalated phenyl rings are several times larger than similar compounds with thiophene or benzothiophene aryl groups. As a result, the first choice for this study was the C^N ligand pphen, a more conjugated analogue of piq. This C^N ligand and close derivatives had previously been used to support deep-red-phosphorescent Ir(pphen)$_2$(L^X) compounds with 2-picolinate or acac ancillary ligands, with peak emission wavelengths ~650 nm and a solution Φ_{PL} of 0.27 for the 2-picolinate complex (Table S1).[43,59,60] We reasoned that the more electron-rich ancillary ligands would red-shift the phosphorescence into the DR-NIR, which is indeed what we observe, as all of the pphen complexes **1**–**3** have peak wavelengths > 700 nm in THF, and all but **1** (λ_{em} = 694 nm) are beyond 700 nm in toluene. The beneficial effects of the acNac ancillary ligand in **1** are apparent; despite the 45 nm (1000 cm^{-1}) red-shift relative to the 2-picolinate analogue,[43] the photoluminescence quantum yield remains at 0.27 in toluene.

Normally such a red shift would cause a decrease in Φ_{PL}, per the energy gap law.[37]

Even better outcomes were obtained with the C^N ligand piqCN, an analogue of piq with a cyano group at the 4-position of the isoquinoline heterocycle. This C^N ligand had previously been used to support Ir(piqCN)$_2$(acac), reported to luminesce at 696 nm with Φ_{PL} = 0.16 (Table S1).[34] We observe a significant red-shift deeper into the DR-NIR *and* a substantial increase in Φ_{PL} for Ir(piqCN)$_2$(acNac) (**4**) and Ir(piqCN)$_2$(dipba^{mes}) (**6**). In **4** the peak wavelength red-shifts by 13 nm (260 cm^{-1}) and the quantum yield more than triples (0.53 vs. 0.16) relative to the acac analogue. In **6**, the electron-rich amidinate ligand results in a peak PL wavelength of 749 nm, further into the DR-NIR than other piqCN or btph complexes, and the quantum yield is maintained at a very good value of 0.30. In short, complexes **4** and **6** have some of the highest reported Φ_{PL} values for cyclometalated iridium complexes which phosphoresce in their respective regions of the spectrum.

The electronic effects of the L^X ligands are similar to those observed in red-phosphorescent analogues,[39] and we believe they are related to the high DR-NIR phosphorescence efficiencies in the compounds described here, particularly **1**, **4**, and **6**. As the CV data in Fig. 2 shows, the electron-rich ancillary ligands destabilize the HOMO, which has significant Ir 5*d*π character. The Ir^{IV}/Ir^{III} redox potentials in **1–6** are at least 0.3 V more negative than the respective acac or 2-picolinate complex with the same C^N ligand,[34,43] whereas the reduction potentials and associated LUMO energies are much less affected. As a result, the estimated HOMO–LUMO gaps in **1–6** are at least 0.2 eV smaller than the acac or 2-picolinate analogues, which in turn stabilizes the charge-transfer states that result from HOMO→LUMO or other Ir 5*d*π→C^N π* transitions. Normally the radiative rate constant is higher with more excited-state MLCT character, as a result of increased spin-orbit coupling,[47] so this stabilization of charge-transfer states, which involve significant MLCT character, can result in higher Φ_{PL} values. Interestingly, the reference compound Ir(piqCN)$_2$(acac) is reported to have an exceptionally high k_r value (1.1×10^6 s^{-1} in THF solution),[34] and the compounds reported here have similar k_r values, meaning it is decreases in k_{nr} that are most important. We have established limited insights into how to control k_{nr} values in this broader class of compounds,[41] and for reasons that are not entirely clear, complexes with L^X = acNac tend to have comparatively low k_{nr} values.[39] Nevertheless, two of the three piqCN compounds have higher quantum yields than the acac analogue, despite their emission being deeper in the DR-NIR region.

We acknowledge that the above comparisons to previous literature precedents are somewhat confounded by solvent effects, which are not discussed in the literature cited above on previous C^N = pphen and piqCN complexes. As part of the current study, we investigated the effects of solvent polarity on the photoluminescence wavelengths and quantum yields and found they can be significant. Luminescence solvatochromism in the new compounds described here depends on the ancillary ligand. The two acNac compounds showed positive solvatochromism in their PL spectra, shifting to longer wavelength as the solvent polarity increases. However, the remaining four compounds with more electron-rich L^X ligands showed irregular solvatochromic behavior, with the longest-wavelength emission occurring in THF, blue-shifting in both MeCN (higher polarity) and toluene (lower polarity). Regardless of the nature of the solvatochromism, we consistently observe photoluminescence quantum yields that are inversely related to the solvent polarity, reaching their maximum values in toluene solvent. By comparing lifetimes in THF and toluene, we find that these higher quantum yields are in most cases a combination of increased k_r and decreased k_{nr} values in the less polar solvent. The origins of these effects are not entirely clear, and they are too large to be explained entirely by energy-gap arguments. However, there are two factors that influence k_r which could be solvent-dependent, the transition-dipole term and spin-orbit coupling. The UV-vis absorption spectra are nearly identical in THF and toluene (see Fig. S11–S22†), so we don't expect a very large solvent dependence of the transition-dipole term although we cannot explicitly rule it out. This suggests that enhanced spin-orbit coupling is involved in the higher k_r values in toluene vs. THF. Spin-orbit coupling in cyclometalated iridium complexes is complex, and primarily involves multiple, closely-spaced MLCT states.[61] MLCT or any other class of charge-transfer states involve significant dipole changes relative to the ground-state, and as such their energies are dependent on solvent polarity. Thus, we believe that the relative energies of one or more coupling states are altered as the solvent changes, which leads to different degrees of spin-orbit coupling that have measurable impacts on k_r.

Conclusions

Here we demonstrated that electron-rich ancillary ligands can lead to more efficient DR-NIR phosphorescence for cyclometalated iridium complexes. We had previously introduced and developed this strategy for red-phosphorescent compounds, and we now show that it is likewise effective at increasing quantum yields in the DR-NIR, a region of the spectrum where it is even more challenging to achieve high-efficiency luminescence. We introduced six novel bis-cyclometalated iridium near-infrared phosphorescent emitters, which in all cases have phosphorescence deeper in the DR-NIR than related compounds with the same C^N ligands. In three of the compounds this profound red shift is accompanied by a quantum yield that rivals or exceeds that of other state-of-the-art DR-NIR iridium phosphors. The electrochemical and photophysical properties indicate significant impacts of the electron-rich ancillary ligand on frontier orbital energies and the excited-state energy landscape, which we believe are responsible for the enhancement in DR-NIR phosphorescence we see in some of these complexes. Efficient DR-NIR phosphors are important for applications that include bioimaging and data security, and this work reveals important fundamental insights into how to control and optimize phosphorescence in the DR-NIR region, beyond 700 nm.

Experimental

Additional details are provided in the ESI†. Brief, representative procedures are provided below.

Preparation of complexes 1–6. The chloro-bridged dimer $[Ir(C^N)_2(\mu\text{-}Cl)]_2$ (C^N = pphen or piqCN) and the potassium or lithium salt of the respective L^X ligand were combined in THF or toluene. The reaction mixture was stirred for 12–48 h at room temperature or heated to 85 °C overnight (L^X = dipba^{mes}). After removing the solvent under reduced pressure, the crude product was extracted into toluene and filtered. The solvent was removed again, and the resulting product was further purified by extracting into THF/pentane, precipitating from THF/pentane, and/or or washing with Et_2O and hexane. After drying in vacuo, isolated yields of 25–60% were obtained.

Photophysical measurements. UV-vis absorption spectra were recorded in THF solutions in screw-capped quartz cuvettes using an Agilent Carey 8454 UV−vis spectrophotometer. Luminescence lifetimes were measured with a Horiba DeltaFlex Lifetime System, using 455 nm pulsed diode excitation. Steady-state emission spectra were recorded using a Horiba FluoroMax-4 spectrofluorometer with appropriate long-pass filters to exclude stray excitation light from detection. In order to exclude air, samples for emission spectra were prepared in a nitrogen-filled glovebox using anhydrous solvents. Solution quantum yields were determined relative to a standard of tetraphenylporphyrin in toluene, which has a reported fluorescence quantum yield (Φ_F) of 0.11.[62] Quantum yields of PMMA film samples were recorded with an integrating sphere.

Author Contributions

Sungwon Yoon: conceptualization, formal analysis, investigation, visualization, writing – original draft, writing – review & editing. Thomas S. Teets: conceptualization, formal analysis, project administration, supervision, visualization, writing – review & editing.

Conflicts of interest

There are no conflicts to declare.

Acknowledgements

We thank the National Science Foundation (Grant No. CHE-1846831) and the Welch Foundation (Grant No. E-1887) for funding this research.

Notes and references

§ **1**·$2CH_2Cl_2$·$0.25C_6H_{14}$: CCDC 2166715, $C_{52.50}H_{43.50}Cl_4IrN_3O$, M = 1066.40, Monoclinic, $P2_1/c$, a = 16.734(2) Å, b = 18.670(2) Å, c = 14.2497(17) Å, β = 93.064(1)°, Z = 4, 62444 tot. refln., 10316 ind. refln., R_{int} = 0.036, R_1 = 0.022, wR_2 = 0.062. **6**·C_4H_8O·C_5H_{12}: CCDC 2166716, $C_{57}H_{63}IrN_6O$, M = 1040.33, Triclinic, P-1, a = 11.9943(10) Å, b = 12.8259(11) Å, c = 17.1312(14) Å, α = 101.445(1) °, β = 107.231(1), γ = 98.910(1)°, Z = 2, 57884 tot. refln., 10583 ind. refln., R_{int} = 0.025, R_1 = 0.018, wR_2 = 0.049.

1 M. Vasilopoulou, A. Fakharuddin, F. P. García de Arquer, D. G. Georgiadou, H. Kim, Abd. R. bin Mohd Yusoff, F. Gao, M. K. Nazeeruddin, H. J. Bolink and E. H. Sargent, Advances in solution-processed near-infrared light-emitting diodes, *Nat. Photonics*, 2021, **15**, 656–669.

2 J. Clark and G. Lanzani, Organic photonics for communications, *Nat. Photonics*, 2010, **4**, 438–446.

3 A. L. Antaris, H. Chen, K. Cheng, Y. Sun, G. Hong, C. Qu, S. Diao, Z. Deng, X. Hu, B. Zhang, X. Zhang, O. K. Yaghi, Z. R. Alamparambil, X. Hong, Z. Cheng and H. Dai, A small-molecule dye for NIR-II imaging, *Nat. Mater.*, 2016, **15**, 235–242.

4 C. Jin, R. Guan, J. Wu, B. Yuan, L. Wang, J. Huang, H. Wang, L. Ji and H. Chao, Rational design of NIR-emitting iridium(III) complexes for multimodal phosphorescence imaging of mitochondria under two-photon excitation, *Chem. Commun.*, 2017, **53**, 10374–10377.

5 E. J. Peterson, W. Qi, I. N. Stanton, P. Zhang and M. J. Therien, Driving high quantum yield NIR emission through proquinoidal linkage motifs in conjugated supermolecular arrays, *Chem. Sci.*, 2020, **11**, 8095–8104.

6 Y. Zhang, Y. Wang, J. Song, J. Qu, B. Li, W. Zhu and W.-Y. Wong, Near-Infrared Emitting Materials via Harvesting Triplet Excitons: Molecular Design, Properties, and Application in Organic Light Emitting Diodes, *Adv. Opt. Mater.*, 2018, **6**, 1800466.

7 Q. Yang, H. Jin, Y. Gao, J. Lin, H. Yang and S. Yang, Photostable Iridium(III)–Cyanine Complex Nanoparticles for Photoacoustic Imaging Guided Near-Infrared Photodynamic Therapy in Vivo, *ACS Appl. Mater. Interfaces*, 2019, **11**, 15417–15425.

8 P.-Y. Ho, C.-L. Ho and W.-Y. Wong, Recent advances of iridium(III) metallophosphors for health-related applications, *Coord. Chem. Rev.*, 2020, **413**, 213267.

9 X. Zhao, Y. Li, D. Jin, Y. Xing, X. Yan and L. Chen, A near-infrared multifunctional fluorescent probe with an inherent tumor-targeting property for bioimaging, *Chem. Commun.*, 2015, **51**, 11721–11724.

10 F. D. Duman, I. Hocaoglu, D. G. Ozturk, D. Gozuacik, A. Kiraz and H. Yagci Acar, Highly luminescent and cytocompatible cationic Ag2S NIR-emitting quantum dots for optical imaging and gene transfection, *Nanoscale*, 2015, **7**, 11352–11362.

11 M. Lin, Y. Zhao, S. Wang, M. Liu, Z. Duan, Y. Chen, F. Li, F. Xu and T. Lu, Recent advances in synthesis and surface modification of lanthanide-doped upconversion nanoparticles for biomedical applications, *Biotechnol. Adv.*, 2012, **30**, 1551–1561.

12 A. Breivogel, C. Kreitner and K. Heinze, Redox and Photochemistry of Bis(terpyridine)ruthenium(II) Amino Acids and Their Amide Conjugates – from Understanding to Applications, *Eur. J. Inorg. Chem.*, 2014, **2014**, 5468–5490.

13 X. Yang, H. Guo, X. Xu, Y. Sun, G. Zhou, W. Ma and Z. Wu, Enhancing Molecular Aggregations by Intermolecular Hydrogen Bonds to Develop Phosphorescent Emitters for High-Performance Near-Infrared OLEDs, *Adv. Sci.*, 2019, **6**, 1801930.

14 K. Tuong Ly, R.-W. Chen-Cheng, H.-W. Lin, Y.-J. Shiau, S.-H. Liu, P.-T. Chou, C.-S. Tsao, Y.-C. Huang and Y. Chi, Near-infrared organic light-emitting diodes with very high external quantum efficiency and radiance, *Nat. Photonics*, 2017, **11**, 63–68.

15 J.-L. Liao, Y. Chi, C.-C. Yeh, H.-C. Kao, C.-H. Chang, M. A. Fox, P. J. Low and G.-H. Lee, Near infrared-emitting tris-bidentate Os(II) phosphors: control of excited state characteristics and fabrication of OLEDs, *J. Mater. Chem. C*, 2015, **3**, 4910–4920.

16 Y. Yuan, J.-L. Liao, S.-F. Ni, A. K.-Y. Jen, C.-S. Lee and Y. Chi, Boosting Efficiency of Near-Infrared Organic Light-Emitting Diodes with Os(II)-Based Pyrazinyl Azolate Emitters, *Adv. Funct. Mater.*, 2020, **30**, 1906738.

17 X. Yang, Y. Zhang, L. Cao, M. Shao, J. Cao, J. Yu, H. Tan and W. Zhu, Achieving near-infrared emission platinum(II) complex by introducing dimerized benzothiadiazole unit, *Opt. Mater.*, 2022, **123**, 111896.

18 S. Roy, A. A. Lopez, J. E. Yarnell and F. N. Castellano, Metal–Metal-to-Ligand Charge Transfer in Pt(II) Dimers Bridged by Pyridyl and Quinoline Thiols, *Inorg. Chem.*, 2022, **61**, 121–130.
19 S. F. Wang, L.-W. Fu, Y.-C. Wei, S.-H. Liu, J.-A. Lin, G.-H. Lee, P.-T. Chou, J.-Z. Huang, C.-I. Wu, Y. Yuan, C.-S. Lee and Y. Chi, Near-Infrared Emission Induced by Shortened Pt–Pt Contact: Diplatinum(II) Complexes with Pyridyl Pyrimidinato Cyclometalates, *Inorg. Chem.*, 2019, **58**, 13892–13901.
20 S. Otto, M. Grabolle, C. Förster, C. Kreitner, U. Resch-Genger and K. Heinze, $[Cr(ddpd)_2]^{3+}$: A Molecular, Water-Soluble, Highly NIR-Emissive Ruby Analogue, *Angew. Chem. Int. Ed.*, 2015, **54**, 11572–11576.
21 F. Reichenauer, C. Wang, C. Förster, P. Boden, N. Ugur, R. Báez-Cruz, J. Kalmbach, L. M. Carrella, E. Rentschler, C. Ramanan, G. Niedner-Schatteburg, M. Gerhards, M. Seitz, U. Resch-Genger and K. Heinze, Strongly Red-Emissive Molecular Ruby $[Cr(bpmp)_2]^{3+}$ Surpasses $[Ru(bpy)_3]^{2+}$, *J. Am. Chem. Soc.*, 2021, **143**, 11843–11855.
22 W. R. Kitzmann, C. Ramanan, R. Naumann and K. Heinze, Molecular ruby: exploring the excited state landscape, *Dalton Trans.*, 2022, **51**, 6519–6525.
23 X. Wang and O. S. Wolfbeis, Optical methods for sensing and imaging oxygen: materials, spectroscopies and applications, *Chem. Soc. Rev.*, 2014, **43**, 3666–3761.
24 J.-H. Shon, S. Sittel and T. S. Teets, Synthesis and Characterization of Strong Cyclometalated Iridium Photoreductants for Application in Photocatalytic Aryl Bromide Hydrodebromination, *ACS Catal.*, 2019, **9**, 8646–8658.
25 R. D. Costa, E. Ortí, H. J. Bolink, F. Monti, G. Accorsi and N. Armaroli, Luminescent Ionic Transition-Metal Complexes for Light-Emitting Electrochemical Cells, *Angew. Chem. Int. Ed.*, 2012, **51**, 8178–8211.
26 M. A. Baldo, D. F. O'Brien, Y. You, A. Shoustikov, S. Sibley, M. E. Thompson and S. R. Forrest, Highly efficient phosphorescent emission from organic electroluminescent devices, *Nature*, 1998, **395**, 151–154.
27 S. Lamansky, P. Djurovich, D. Murphy, F. Abdel-Razzaq, H.-E. Lee, C. Adachi, P. E. Burrows, S. R. Forrest and M. E. Thompson, Highly Phosphorescent Bis-Cyclometalated Iridium Complexes: Synthesis, Photophysical Characterization, and Use in Organic Light Emitting Diodes, *J. Am. Chem. Soc.*, 2001, **123**, 4304–4312.
28 S. Baek, S.-Y. Kwak, S.-T. Kim, K. Y. Hwang, H. Koo, W.-J. Son, B. Choi, S. Kim, H. Choi and M.-H. Baik, Ancillary ligand increases the efficiency of heteroleptic Ir-based triplet emitters in OLED devices, *Nat. Commun.*, 2020, **11**, 2292.
29 W. Li, B. Wang, T. Miao, J. Liu, X. Lü, G. Fu, L. Shi, Z. Chen, P. Qian and W.-Y. Wong, C1-Symmetric [Ir(C^N1)(C^N2)(O^O)]-Tris-Heteroleptic Iridium(III)-Complexes with the Preferentially Horizontal Orientation for High-Performance Near-Infrared Organic Light-Emitting Diodes, *Adv. Opt. Mater.*, 2021, **9**, 2100117.
30 Q. Zhao, C. Huang and F. Li, Phosphorescent heavy-metal complexes for bioimaging, *Chem. Soc. Rev.*, 2011, **40**, 2508–2524.
31 A. Tsuboyama, H. Iwawaki, M. Furugori, T. Mukaide, J. Kamatani, S. Igawa, T. Moriyama, S. Miura, T. Takiguchi, S. Okada, M. Hoshino and K. Ueno, Homoleptic Cyclometalated Iridium Complexes with Highly Efficient Red Phosphorescence and Application to Organic Light-Emitting Diode, *J. Am. Chem. Soc.*, 2003, **125**, 12971–12979.
32 C.-H. Fan, P. Sun, T.-H. Su and C.-H. Cheng, Host and Dopant Materials for Idealized Deep-Red Organic Electrophosphorescence Devices, *Adv. Mater.*, 2011, **23**, 2981–2985.
33 T. Yoshihara, S. Murayama, T. Masuda, T. Kikuchi, K. Yoshida, M. Hosaka and S. Tobita, Mitochondria-targeted oxygen probes based on cationic iridium complexes with a 5-amino-1, 10-phenanthroline ligand, *J. Photochem. Photobiol. Chem.*, 2015, **299**, 172–182.
34 Z. Chen, H. Zhang, D. Wen, W. Wu, Q. Zeng, S. Chen and W.-Y. Wong, A simple and efficient approach toward deep-red to near-infrared-emitting iridium(III) complexes for organic light-emitting diodes with external quantum efficiencies of over 10%, *Chem. Sci.*, 2020, **11**, 2342–2349.
35 C. You, D. Liu, J. Yu, H. Tan, M. Zhu, B. Zhang, Y. Liu, Y. Wang and W. Zhu, Boosting Efficiency of Near-Infrared Emitting Iridium(III) Phosphors by Administrating Their π–π Conjugation Effect of Core–Shell Structure in Solution-Processed OLEDs, *Adv. Opt. Mater.*, 2020, **8**, 2000154.
36 K. F. Freed and J. Jortner, Multiphonon Processes in the Nonradiative Decay of Large Molecules, *J. Chem. Phys.*, 1970, **52**, 6272–6291.
37 R. Englman and J. Jortner, The energy gap law for radiationless transitions in large molecules, *Mol. Phys.*, 1970, **18**, 145–164.
38 H. Yersin, in *Highly efficient OLEDs with phosphorescent materials*, WILEY-VCH, Weinheim, 2008, pp. 1–97.
39 P.-N. Lai, C. H. Brysacz, M. K. Alam, N. A. Ayoub, T. G. Gray, J. Bao and T. S. Teets, Highly Efficient Red-Emitting Bis-Cyclometalated Iridium Complexes, *J. Am. Chem. Soc.*, 2018, **140**, 10198–10207.
40 P. Lai and T. S. Teets, Ancillary Ligand Effects on Red-Emitting Cyclometalated Iridium Complexes, *Chem. – Eur. J.*, 2019, **25**, 6026–6037.
41 E. Kabir, Y. Wu, S. Sittel, B.-L. Nguyen and T. S. Teets, Improved deep-red phosphorescence in cyclometalated iridium complexes *via* ancillary ligand modification, *Inorg. Chem. Front.*, 2020, **7**, 1362–1373.
42 P. Lai, S. Yoon, Y. Wu and T. S. Teets, Effects of Ancillary Ligands on Deep Red to Near-Infrared Cyclometalated Iridium Complexes, *ACS Org. Inorg. Au*, 2022, **2**, 236–244.
43 J. M. Fernandez-Hernandez, E. Longhi, R. Cysewski, F. Polo, H.-P. Josel and L. De Cola, Photophysics and Electrochemiluminescence of Bright Cyclometalated Ir(III) Complexes in Aqueous Solutions, *Anal. Chem.*, 2016, **88**, 4174–4178.
44 Y. K. Radwan, A. Maity and T. S. Teets, Manipulating the Excited States of Cyclometalated Iridium Complexes with β-Ketoiminate and β-Diketiminate Ligands, *Inorg. Chem.*, 2015, **54**, 7122–7131.
45 R. A. Maya, A. Maity and T. S. Teets, Fluorination of Cyclometalated Iridium β-Ketoiminate and β-Diketiminate Complexes: Extreme Redox Tuning and Ligand-Centered Excited States, *Organometallics*, 2016, **35**, 2890–2899.
46 P.-N. Lai, S. Yoon and T. S. Teets, Efficient near-infrared luminescence from bis-cyclometalated iridium(III) complexes with rigid quinoline-derived ancillary ligands, *Chem. Commun.*, 2020, **56**, 8754–8757.
47 H. Yersin, A. F. Rausch, R. Czerwieniec, T. Hofbeck and T. Fischer, The triplet state of organo-transition metal compounds. Triplet harvesting and singlet harvesting for efficient OLEDs, *Coord. Chem. Rev.*, 2011, **255**, 2622–2652.
48 E. M. Espinoza, J. A. Clark, J. Soliman, J. B. Derr, M. Morales and V. I. Vullev, Practical Aspects of Cyclic Voltammetry: How to Estimate Reduction Potentials When Irreversibility Prevails, *J. Electrochem. Soc.*, 2019, **166**, H3175–H3187.
49 P. I. Djurovich, E. I. Mayo, S. R. Forrest and M. E. Thompson, Measurement of the lowest unoccupied molecular orbital energies of molecular organic semiconductors, *Org. Electron.*, 2009, **10**, 515–520.
50 J. Pommerehne, H. Vestweber, W. Guss, R. F. Mahrt, H. Bässler, M. Porsch and J. Daub, Efficient two layer leds on a polymer blend basis, *Adv. Mater.*, 1995, **7**, 551–554.
51 S. Lamansky, P. Djurovich, D. Murphy, F. Abdel-Razzaq, R. Kwong, I. Tsyba, M. Bortz, B. Mui, R. Bau and M. E. Thompson, Synthesis and Characterization of Phosphorescent Cyclometalated Iridium Complexes, *Inorg. Chem.*, 2001, **40**, 1704–1711.

52 A. Beeby, S. Bettington, I. D. W. Samuel and Z. Wang, Tuning the emission of cyclometalated iridium complexes by simple ligand modification, *J. Mater. Chem.*, 2003, **13**, 80–83.
53 Y. You and S. Y. Park, Inter-Ligand Energy Transfer and Related Emission Change in the Cyclometalated Heteroleptic Iridium Complex: Facile and Efficient Color Tuning over the Whole Visible Range by the Ancillary Ligand Structure, *J. Am. Chem. Soc.*, 2005, **127**, 12438–12439.
54 J. R. Lakowicz, in *Principles of fluorescence spectroscopy*, Springer, New York, 3rd ed., 2006, pp. 205–235.
55 S. Nigam and S. Rutan, Principles and Applications of Solvatochromism, *Appl. Spectrosc.*, 2001, **55**, 362A-370A.
56 P. G. Seybold and M. Gouterman, Porphyrins, *J. Mol. Spectrosc.*, 1969, **31**, 1–13.
57 C.-L. Ho, H. Li and W.-Y. Wong, Red to near-infrared organometallic phosphorescent dyes for OLED applications, *J. Organomet. Chem.*, 2014, **751**, 261–285.
58 A. J. Lees, The Luminescence Rigidochromic Effect Exhibited by Organometallic Complexes: Rationale and Applications, *Comments Inorg. Chem.*, 1995, **17**, 319–346.
59 E. Longhi, J. M. Fernandez-Hernandez, A. Iordache, R. Fröhlich, H.-P. Josel and L. De Cola, Ir(III) Cyclometalated Complexes Containing Phenylphenanthridine Ligands with Different Substitutions: Effects on the Electrochemiluminescence Properties, *Inorg. Chem.*, 2020, **59**, 7435–7443.
54 B. Jiang, Y. Gu, J. Qin, X. Ning, S. Gong, G. Xie and C. Yang, Deep-red iridium(III) complexes cyclometalated by phenanthridine derivatives for highly efficient solution-processed organic light-emitting diodes, *J. Mater. Chem. C*, 2016, **4**, 3492–3498.
61 E. Zysman-Colman, Ed., *Iridium(III) in Optoelectronic and Photonics Applications*, John Wiley & Sons, Inc, Chichester, West Sussex, 2017.
62 P. G. Seybold and M. Gouterman, Porphyrins: XIII: Fluorescence spectra and quantum yields, *J. Mol. Spectrosc.*, 1969, **31**, 1–13.